Optical transparency by detuned electrical dipoles

New Journal of Physics
The open-access journal for physics

Optical transparency by detuned electrical dipoles

Sergey I Bozhevolnyi[1,4], Andrey B Evlyukhin[2], Anders Pors[3], Michael G Nielsen[1], Morten Willatzen[3] and Ole Albrektsen[1]

[1] Institute of Sensors, Signals and Electrotechnics (SENSE), University of Southern Denmark, Niels Bohrs Allé 1, DK-5230 Odense M, Denmark
[2] Laser Zentrum Hannover eV, Hollerithallee 8, D-30419 Hannover, Germany
[3] Mads Clausen Institute (MCI), University of Southern Denmark, Alsion 2, DK-6400 Sønderborg, Denmark
E-mail: seib@sense.sdu.dk

New Journal of Physics **13** (2011) 023034 (20pp)
Received 8 November 2010
Published 21 February 2011
Online at http://www.njp.org/
doi:10.1088/1367-2630/13/2/023034

Abstract. We demonstrate that optical transparency can be realized with plasmonic metamaterials using unit cells consisting of detuned electrical dipoles (DED), thereby mimicking the dressed-state picture of the electromagnetically induced transparency (EIT) in atomic physics. Theoretically analyzing the DED cells with two and three different silver ellipsoids, we show the possibility of reaching a $\geqslant$10 times decrease in group velocity and a propagation loss of $\leqslant$1 dB per cell within the optical wavelength range of 625–640 nm. Similar configurations are realized with lithographically fabricated gold nanorods placed on a glass substrate and subsequently covered with a $\sim$15-μm-thick polymer layer, featuring EIT-like transmission spectra with transparency windows at wavelengths of $\sim$850 nm.

[4] Author to whom any correspondence should be addressed.

Contents

1. Introduction **2**
2. Detuned electrical dipoles (DED)-based optical transparency **4**
3. DED metamaterials using silver nanoparticles **5**
3.1. Two-particle DED configuration 5
3.2. Three-particle DED configuration 10
4. DED metamaterials using gold nanorods **10**
4.1. Two-nanorod DED configuration 11
4.2. Three-nanorod DED configuration 13
4.3. Nanorod-based DED metamaterials 15
5. Preliminary experiments **17**
6. Conclusions **18**
Acknowledgments **19**
References **20**

1. Introduction

The phenomenon of electromagnetically induced transparency (EIT) is based on the laser-induced coherence of atomic states leading to quantum interference between the excitation pathways controlling the optical response, which is thereby modified exhibiting enhanced transmission [1, 2]. The strongly enhanced transmission within the absorption band results in strong dispersion and consequently in a significant reduction in the group velocity (see e.g. [2] and references therein). Slowing down the propagation of light pulses enhances light–matter interactions, allowing one, for example, to boost optical nonlinearities and to tackle the tantalizing problem of an all-optical buffer [3]. Realization of the EIT-like response with classical oscillator systems has been reported for a number of photonic configurations involving coupled optical resonators [4]–[9], so that the phenomenon in question is often called coupled-resonator-induced transparency (CRIT) [5, 10]. Very recently, it was shown that the CRIT principle can also be implemented using plasmonic resonators in the form of metal nanostrip antennas [11]. However, since the dimensions of CRIT configurations are principally of the order of a light wavelength, other approaches should be explored in order to realize an *effective medium* composed of subwavelength unit cells (i.e. metamaterial) exhibiting the EIT-like behavior. Recently, the idea of EIT realization with electromagnetic metamaterials has been exploited in several configurations [12]–[16], including metamaterials consisting of plasmonic 'molecules', i.e. metal nanostructures whose plasmon-driven responses mimic those of atomic EIT systems [12, 15]. Note that the Fano resonances in plasmonic nanostructures and metamaterials intensively investigated over the last few years can be viewed, under certain conditions, as the classical manifestation of EIT [17]. Considering the slow-light phenomenon associated with EIT, it should be emphasized that slowing light down, which requires very strong dispersion of propagating waves, can be realized via strong *material* dispersion (e.g. achieved with EIT) or by using the *geometrical* dispersion arising in engineered structures (e.g. in the aforementioned photonic configurations and metamaterials as well as in photonic crystals [18]).

The phenomenon of EIT can be considered in two alternative ways: as resulting from the destructive interference between two pathways involving either the *bare*, dipole-allowed and metastable states or, *equivalently*, the doublet of *dressed* states (created by strong pump radiation) representing two closely spaced resonances decaying to the same continuum [1, 2]. While these two physical pictures are equivalent when dealing with EIT in atomic systems, their realization with plasmonic nanostructures, whose responses are determined by their configurations and *not* electromagnetically induced as in EIT, *depends* on the EIT mechanism that is imitated. The first picture suggests employing radiative and subradiant (dark) plasmonic elements that are strongly coupled by being closely placed and appropriately oriented [12, 15]. Note that the strong-coupling condition imposes rather stringent requirements on the fabrication accuracy for the plasmonic structures to be operated at optical wavelengths [12]. Alternatively viewed, EIT is achieved due to the cancellation of opposite contributions from two resonances, which are equally spaced but with opposite signs of detuning from the probe frequency, due to the Fano-like interference of the decay channels. Fundamentally, the dressed-state picture of EIT is equivalent to the case of interference between two closely spaced lifetime-broadened resonances decaying to the same continuum [1]. The underlying physics of the cancellation of absorption in EIT is also similar to that involved in the phenomenon of coherent population trapping [2]. Metamaterials utilizing trapped-mode resonances and featuring the EIT-like transmission spectra have been realized in the cm-wavelength range using fish-scale patterns [13] and concentric ring resonators [16]. In both configurations, electrical currents induced (at the trapped-mode resonance frequency) in different parts of a unit cell oscillate with opposite phases, resulting in scattering suppression and enhanced transmission.

It should be emphasized that the EIT realization with *plasmonic* nanostructures is *fundamentally* different from EIT in atomic systems with respect to the linewidths of resonances involved: while atomic resonances are lifetime broadened, the linewidth of plasmonic resonances is determined not only by radiation damping but also by absorption, i.e. by direct *loss* of photons. In this case, the EIT phenomenon manifests itself as the *scattering suppression*, whereas the absorption (becoming progressively more important and even dominant at optical frequencies) is mainly determined by the fundamental material properties and is *impossible* to eliminate no matter which EIT realization approach is chosen [19]. For this reason, one should not expect to achieve *complete* transparency when dealing with plasmonic nanostructures, as also seen from the reported simulations [11, 12] and experiments [15].

We have recently investigated the optical properties of periodic arrays of pairs of gold nanorods having different lengths and found that these arrays can advantageously be used for very sensitive monitoring of environmental refractive index, i.e. for plasmonic sensing [20]. Essentially, such a nanorod pair represents two dipolar scatterers resonating at different frequencies, i.e. detuned electrical dipoles (DED), whose detuning is simply determined by their difference in length. We have also noted that the transmission spectra exhibited windows of enhanced transmission surrounded on both sides by transmission minima, a phenomenon that we have attributed to the effect of optical transparency that emulates the dressed-state picture of EIT [20]. In this paper, we consider this intriguing effect from different viewpoints in detail, starting with a qualitative picture supported by numerical modeling of DED configurations consisting of silver nanoparticles in air (so as to directly compare our configuration with that reported previously [12]), followed by finite-element simulations of gold nanorods whose results can be compared to those obtained in our preliminary experiments.

2. Detuned electrical dipoles (DED)-based optical transparency

Our approach can be illustrated by considering a metamaterial with the unit cell consisting of two nearly identical and *non-interacting* electric dipolar scatterers, whose resonances are equally detuned from the central frequency ω_0 so that their dipole polarizabilities can be represented as

$$\alpha_{1(2)}(\omega) = \frac{A\omega_0^2}{(\omega_0 \pm \Delta)^2 - \omega^2 - \mathrm{i}\Gamma\omega}, \tag{1}$$

where Δ is the DED detuning frequency, Γ is the damping factor and A characterizes their strength [20]. This type of polarizabilities can readily be implemented in plasmonics for optical frequencies, e.g. with metal nanoshells or nanorods whose resonances can be adjusted by tuning the shell inner-to-outer radius ratio [21] or the rod aspect ratio [22], respectively. In the effective-medium theory (EMT) with the unit cell being much smaller than the light wavelength (see e.g. [23] and references therein), the response of the unit cell is determined (*irrespective* of the dipole positions) by the sum of two polarizabilities, $\alpha_1 + \alpha_2$. For frequencies close to the central frequency, $\delta = \omega - \omega_0 \ll \omega_0$, and weak detuning and damping ($\omega_0 \gg \Delta$, $\Gamma \gg \delta$), the DED response can be expressed with the first-order approximation as (see equation (1))

$$\alpha_1 + \alpha_2 \simeq 2A\omega_0 \left[\delta \frac{2(4\Delta^2 - \Gamma^2)}{(4\Delta^2 + \Gamma^2)^2} + \mathrm{i}\frac{\Gamma}{4\Delta^2 + \Gamma^2}\right], \tag{2}$$

implying strong suppression of scattering, i.e. the regime of optical transparency, at the central frequency ω_0.

In the EMT framework [23], the effective dielectric susceptibility of metamaterials consisting of DED pairs in vacuum (with sufficiently low concentrations N) can be approximated within the transparency window by that of non-interacting unit cells,

$$\varepsilon_{\mathrm{eff}} \simeq 1 + N(\alpha_1 + \alpha_2), \tag{3}$$

because *both* the real and imaginary parts of $\alpha_1 + \alpha_2$ are very small, with both dipoles being *out of resonance* and having *opposite signs* of their real parts of polarizabilities at the central frequency ω_0 (see equation (2)). This makes it possible to directly compare the total polarizability expressed by equation (2) with the susceptibility of an effective medium consisting of plasmonic molecules, in which a radiative element coupled with a subradiant (dark) element (see equation (3) in [12]). One notices that both expressions are similar in form, becoming quantitatively similar if $2\Delta = \kappa$ and $\Gamma^2 \simeq \gamma_a\gamma_b$, where κ is the coupling between the two elements with their damping factors being γ_a and γ_b. Note that the electrostatic limit for quality factors of localized plasmon resonances [24], which is difficult to exceed [25], implies that the latter condition becomes progressively more realistic for optical frequencies because of the dominance of absorption in extinction of plasmonic nanostructures [26].

The aforementioned similarity has a deep physical meaning related to the equivalence of the bare- and dressed-state pictures of the EIT [1, 2]. Mathematically, transformation from the former to the latter occurs by the transition to another (rotating) coordinate system, in which the interaction operator is diagonal. In classical optics, similar equivalence is found, for example, when considering the power exchange between two waveguides in a directional coupler to be a result of the *coupling* between two modes of *individual* waveguides or due to the *interference* of two *super-modes* of a two-waveguide system [27]. In any case, splitting between eigenvalues

of super-modes is proportional to the coupling between two individual oscillators (e.g. in our case: $2\Delta = \kappa$), a feature that is found in many classical and quantum mechanical systems. It is, however, important, from the viewpoint of EIT realization with plasmonic nanostructures, that the *strong-coupling* condition with its stringent fabrication requirements [12, 15] can be traded for the *detuning* condition requiring dipolar scatterers to resonate at different frequencies. The latter seems more amenable to being implemented in practice.

Slowing light down within the transparency window is probably the most striking effect associated with EIT [2]. Using the EMT approach described above (equation (3)) and the condition $N\,\mathrm{Re}(\alpha_1+\alpha_2) \ll 1$ (that can be satisfied near the central frequency (equation (2)), the group index determining the light slowdown can be expressed as

$$n_g \simeq 1 + \frac{\omega N}{2}\frac{\mathrm{dRe}(\alpha_1+\alpha_2)}{\mathrm{d}\omega}. \tag{4}$$

An increase in the group index can thereby be traced to the dispersion of the real part of cell polarizability, resulting in (see equation (2))

$$\left.\frac{\mathrm{d}[\mathrm{Re}(\alpha_1+\alpha_2)]}{\mathrm{d}\omega}\right|_{\omega_0} \simeq 4A\omega_0\frac{4\Delta^2-\Gamma^2}{(4\Delta^2+\Gamma^2)^2}. \tag{5}$$

It should be borne in mind that the group velocity is *generally* not a useful concept in regions of anomalous dispersion [28] and that the above relation should therefore be considered only for relatively large detuning: $\Delta > 0.5\Gamma$. In the case of *normal* dispersion at the probe frequency, one can show that the group refractive index exhibits a broad maximum at $\Delta_{\mathrm{opt}} = \sqrt{0.75}\Gamma$. A similar condition of the detuning to be close to the broadening of two resonances is also found in the dressed-state picture of the EIT for atomic media [1, 2]. Finally, the above condition (equation (5)) being obtained in the approximation of non-interacting dipolar scatterers should be considered only as an *estimate* of the optimum DED detuning, with a careful optimization yet to be conducted for a given DED configuration designed to operate in a given frequency range.

3. DED metamaterials using silver nanoparticles

One of the apparent advantages of the DED configuration from the practical point of view is that it can readily be implemented at any wavelength, also in the visible, because many techniques for fabrication of metal nanoparticles exhibiting prescribed resonance wavelengths have been developed (see e.g. [21, 22]). The above (qualitative) consideration elucidated the basic mechanism of optical transparency in DED-based metamaterials and established an important link to the approach based on coupling between radiative and subradiant plasmonic elements [12, 15]. However, it remains to be seen to what extent the group index increase that can be achieved and the associated propagation loss, especially at optical frequencies, are similar for these two approaches. In this section, we consider DED-based metamaterials utilizing silver nanoparticles being resonant in visible and placed in air so as to directly compare the characteristics of our configuration with those reported previously [12].

3.1. Two-particle DED configuration

We start first with the simplest configuration (type I), in which the unit cell is represented by a pair of ellipsoid silver nanoparticles (figure 1(a)), whose scattering properties are determined by their (electrostatic) dipole polarizabilities [29] calculated using the tabular silver constants [30].

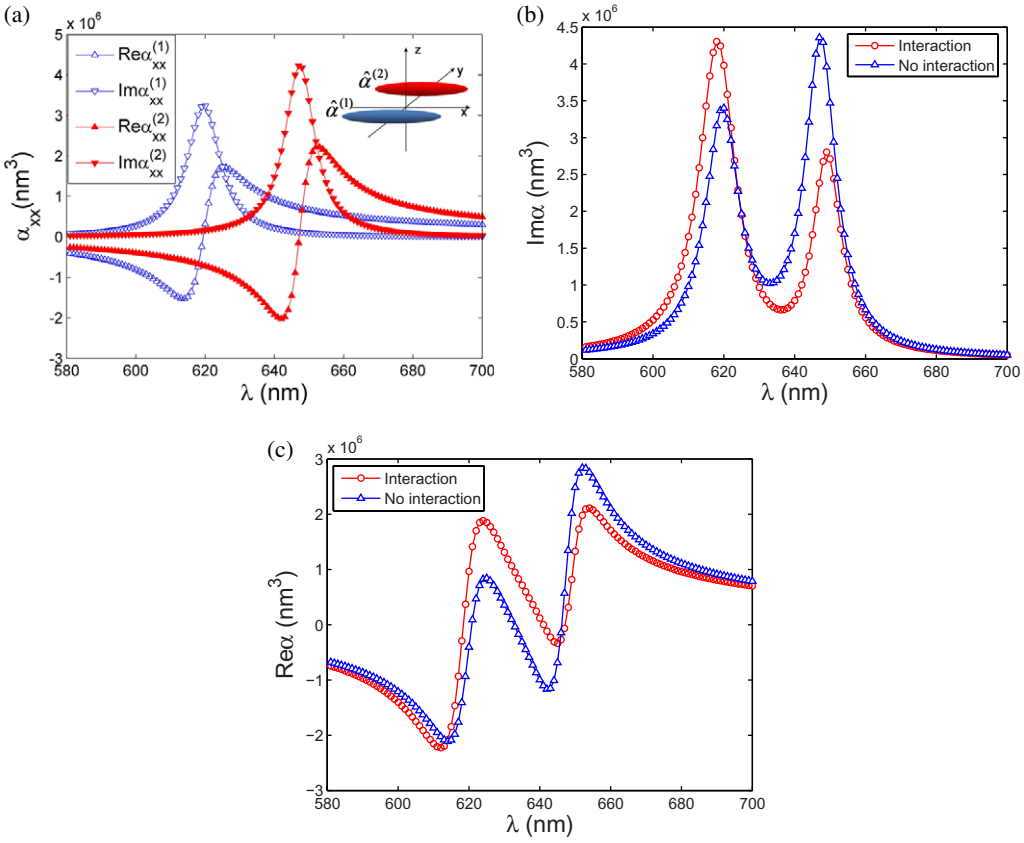

Figure 1. (a) Real and imaginary parts of polarizabilities (for the x-polarized light) of individual silver ellipsoids (in air) with sizes $58.5 \times 11.7 \times 11.7$ and $61.6 \times 11.4 \times 11.4\,\mathrm{nm}^3$ (center-to-center distance of 60 nm), comprising the unit cell of type I (see inset). Spectra of (b) imaginary and (c) real parts of the *total* polarizability (of unit cell) calculated with (red) and without (blue) the dipole interaction being taken into account.

The sizes of ellipsoids were chosen so as to realize, for the x-polarized light, properly detuned resonances of similar strength in the visible (figure 1(a)). The problem of multiple light scattering in the system of two dipolar scatterers was treated self-consistently [29], allowing us to correctly calculate the *total* polaizability of the unit cell, whose real and imaginary parts are displayed (for the x-polarized light), along with those of the cell polarizability for non-interacting dipoles, i.e. $\alpha_1 + \alpha_2$, in figures 1(b) and (c). The idea is to illustrate that the dipole interaction is relatively weak even for the center-to-center distance of $\simeq\lambda/10$, implying that *similar* responses can be obtained with *different* DED separations (non-interacting dipoles are equivalent to extremely separated ones), a remarkable feature of our approach that makes the DED-based metamaterial robust and *non-critical* with respect to fabrication tolerances. It is seen that the general behavior of polarizability spectra is indeed very similar, indicating a minimum in extinction at $\simeq$633 nm surrounded by two maxima (figure 1(b)) along with an increase in the group index related to the dispersion of the real part of the cell polarizability (figure 1(c)). Following the preceding discussion in section 2, one can directly compare the presented spectra of total polarizability (figures 1(a) and (b)) and the spectra reported previously (see figure 2(b)

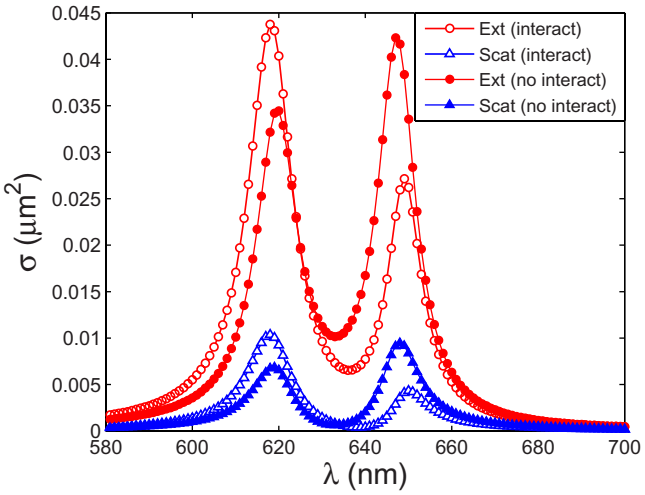

Figure 2. Extinction and scattering cross sections of the single DED cell of type I calculated for the x-polarized incident light with (open symbols) and without (filled symbols) dipole interaction being taken into account.

in [12]), revealing as expected a close resemblance between the general spectral behavior along with a much stronger influence of nanoparticle positioning in the latter case.

The consideration of the properties of the single DED cell is completed with the presentation of its extinction and scattering spectra calculated with and without dipole interaction being taken into account (figure 2). It is seen that, in line with what was discussed in the introduction, the scattering spectra exhibit rather deep minima showing the efficient *scattering suppression* (at least by one order of magnitude for interacting dipoles), whereas the cancellation of extinction is not complete due to the presence of absorption (which is fundamentally determined by the material properties of constituent nanoparticles). It is also seen that the inter-particle interaction results in both red-shifting the extinction and scattering minima (along with red-shifting their maxima) and their noticeable decreases. At the same time, the difference between the two resonance responses becomes more pronounced with the cell response that appears more asymmetric with respect to the extinction minimum (figure 2). These features indicate that, while the inter-dipole interaction might be beneficial (for the considered DED configuration) from the point of view of improving the transparency effect, resonant nanoparticles should not be placed too close to each other to avoid transition from the weak-coupling to strong-coupling regime. Finally, our calculations performed for different DED separations (not shown) have confirmed that even though the inter-dipole interactions are important, influencing the *exact* positions and depths of minima in the scattering and extinction spectra as discussed above, the general behavior of spectra is practically unaffected, as illustrated in figure 2.

We turn now to a consideration of an optical DED-based metamaterial with a unit cell of type I (figure 1(a)). For the unit cell size of $210 \times 210 \times 120\,\mathrm{nm}^3$, the complex amplitude of the transmitted wave was calculated for metamaterials consisting of one to four layers along the propagation direction, i.e. along the z-axis, of the x-polarized incident field, with multiple scattering between all dipolar scatterers being rigorously taken into account [29]. The corresponding transmission spectra (figure 3(a)) exhibit the transmission maximum at

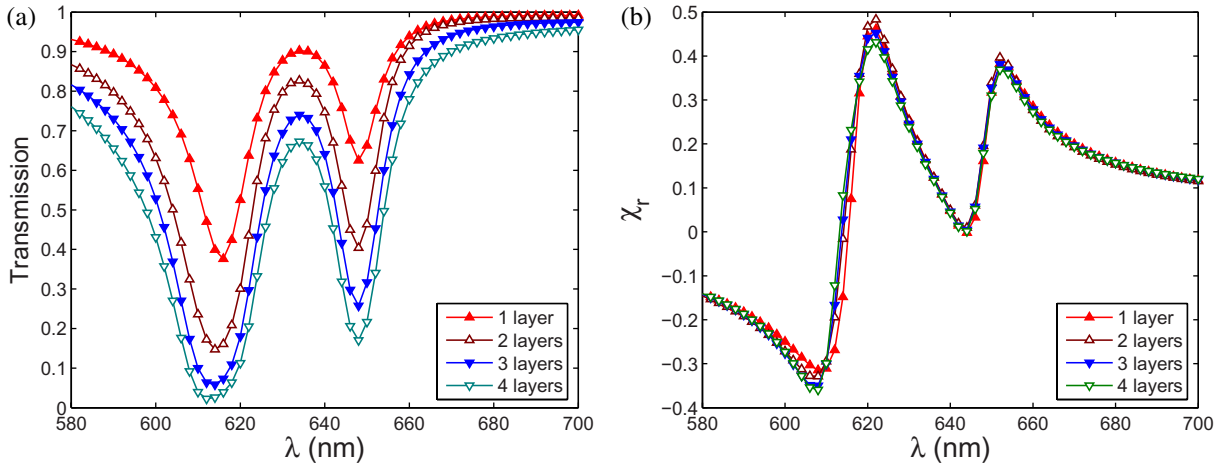

Figure 3. (a) Transmission spectra of optical DED-based metamaterials with the unit cell ($210 \times 210 \times 120\,\mathrm{nm}^3$) of type I for different numbers of layers illuminated with the x-polarized incident light. (b) Corresponding spectra of the real part of effective susceptibility calculated from phase spectra of the transmitted field.

around the central wavelength of $\simeq$633 nm in a broader absorption band, which is similar to the transparency effect observed in the EIT with atomic systems. Similar to what has been previously reported [12], with an increasing number of layers (i.e. with increasing metamaterial thickness), the transparency maximum decreases due to the *inevitable* absorption of radiation by metal nanoparticles. We have also obtained a linear relation between the logarithm of the peak transmission and the number of layers, as expected [12]. The phase of the transmitted field, when being related to that in the case of free space, allows one to determine the real part of effective susceptibility that turned out to be practically independent of the number of layers considered (figure 3(b)), which is a very important characteristic feature of a true optical effective medium [12].

In general, the above results obtained for DED-based metamaterials (figure 3) are directly comparable to those reported for metamaterials based on strongly coupled radiative and dark plasmonic elements (figure 3 in [12]). The central wavelength of $\lambda \simeq 633$ nm, which we have chosen to be in the visible, is somewhat shorter than that of $\simeq$699 nm in [12], but otherwise the transmission and susceptibility spectra are seen to be very much alike for these (principally different) configurations. Consequently, the corresponding metamaterial characteristics relevant to the EIT effect are rather similar as well: the propagation loss of $\simeq$0.3 dB per 120-nm-thick unit cell in our case versus that of $\simeq$0.8 dB per 200-nm-thick unit cell, the transparency bandwidth $\delta\lambda \simeq 15$ nm estimated from the transmission spectra using the excess loss level of 1 dB (figure 3(b)) in our case versus that of $\simeq$19 nm, and the group index $n_g \simeq 7$ estimated from the susceptibility slope (figure 3(b)) versus that of $\simeq$11 [12]. Using these data, one can also estimate the bandwidth-delay product limiting the propagation length L by the loss level of 4.34 dB ($1/e$-level), which amounts to a propagation length of $\simeq 1.74\,\mu$m in our case versus that of $\simeq 1.09\,\mu$m, resulting in the bandwidth-delay product $\tau\Delta f \simeq \lambda^{-2}\delta\lambda L(n_g - 1) \simeq 0.39$ in our case versus that of $\simeq$0.42, both being practically the same and favorably comparable to that calculated using the plasmonic CRIT principle [11]. The above comparison confirms the

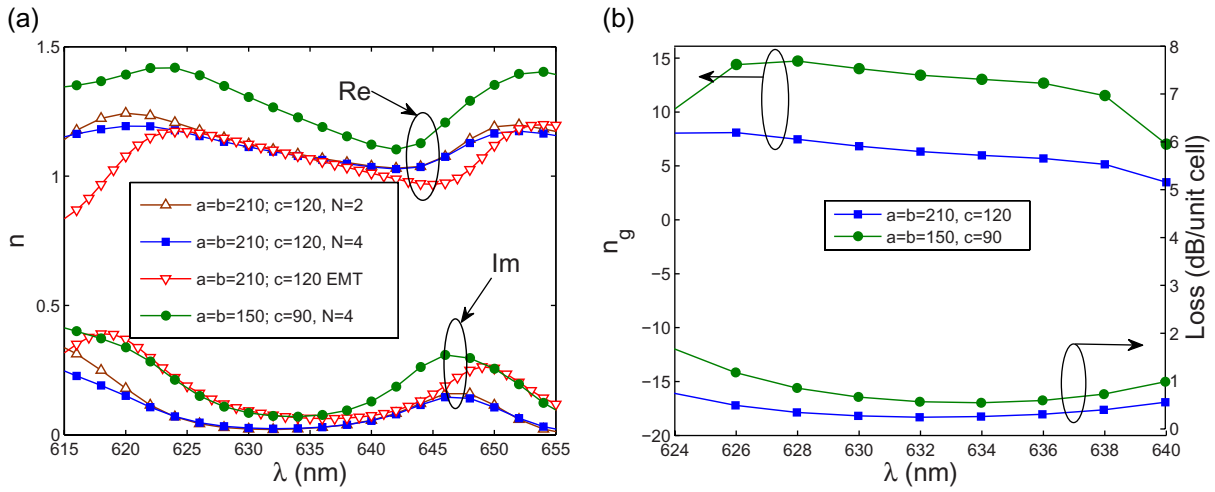

Figure 4. (a) Dispersion of the refractive (real and imaginary parts) index of metamaterials of type I calculated directly from the transmission by 2 and 4 layers of unit cells (a, b and c in the insets indicate the cell dimensions in nanometers along the x-, y- and z-axis, respectively) and by using the EMT for the x-polarized field incident along the z-axis. (b) The corresponding dispersion of the group index and loss per unit cell for DED-based metamaterials of type I for two different unit cells.

qualitative arguments given in section 2 for the *fundamental equivalence* of two plasmonic EIT approaches (DED-based and using strongly coupled radiative and dark elements), which are, however, very different with respect to the fabrication tolerances required.

The dispersion of phase and group indexes for effective media of type I consisting of unit cells of different sizes (figure 4) was calculated both directly by considering several layers of unit cells as described above (figure 3) and with the EMT approach [23] using the total polarizability of a unit cell (figures 1(b) and (c)). Calculations performed for 2 and 4 layers of ellipsoid pairs by retrieving the real and imaginary parts of the refractive index n from the amplitude and phase of the transmitted field [12] agree well (in the domain of normal dispersion) with the EMT for the same cell size (figure 4(a)). It is also seen that a decrease in cell size results in an increase in both the slope of $\mathrm{Re}[n(\lambda)]$ and the metamaterial absorption characterized by $\mathrm{Im}(n)$. The group refractive index and loss (per cell thickness) for different cell sizes (figure 4(b)) were straightforwardly evaluated from the corresponding dependences $n(\lambda)$ (figure 4(a)). It should be stressed again that the group velocity is generally meaningful only in the domain of normal dispersion with relatively small absorption [28], i.e. in the wavelength range of $\sim$625–640 nm in our case. Note that the metamaterial with a smaller (90 nm-thick) unit cell features a significantly higher group index of $\simeq$14, but with a larger loss of $\simeq 0.6$ dB per unit cell in a narrower bandwidth of $\simeq$13 nm. At the same time, the bandwidth-delay product estimated for the propagation length ($1/e$-level) of $\simeq 0.65\,\mu$m amounts to $\simeq$0.27, which is considerably lower (but for a much shorter propagation length) than the value obtained for the metamaterial with a larger unit cell. This comparison shows that optimization of DED-based metamaterials involves not only the proper choice of the DED detuning Δ but also the

dimensions of a unit cell, taking into account other requirements (e.g. insertion loss, thickness and/or the number of layers) as well.

3.2. Three-particle DED configuration

The DED configuration of type I considered above might be somewhat problematic to realize in practice e.g. when using one-step electron-beam lithography, because a shorter resonance wavelength implies typically a shorter nanoparticle [31] and, consequently, a smaller polarizability. At the same time, as follows from qualitative arguments given in section 2, it is important to extinguish at least the real part of the *total* polarizability of a unit cell. Depending on the fabrication technique employed, the latter might be easier to achieve by using *two* small dipolar scatterers resonating at a shorter wavelength being placed on both sides of a large scatterer resonating at a longer wavelength. In this subsection, we consider an example of the metamaterial based on the three-particle DED configuration (type II) of a unit cell.

The main results of the corresponding simulations conducted in the same manner as those reported above for type I are summarized in figure 5. It is seen also for this configuration that, in line with what was discussed in the introduction, the scattering spectra exhibit a very deep minimum, demonstrating the effect of *scattering suppression* by two orders of magnitude. Again, the cancellation of extinction is not complete due to the presence of unavoidable absorption, as discussed above (section 3.1). It is important to note that, despite different cell compositions in type I and II configurations, both cells exhibit very similar EIT-like scattering and extinction spectra when illuminated with the x-polarized light propagating along the z-axis (cf figures 2 and 5(b)). The corresponding metamaterials feature, consequently, similar levels in the group refractive indexes and propagation losses (cf figures 4(b) and 5(c)). At the same time, the metamaterials of type II considered here exhibit a slightly broader transparency bandwidth of $\delta\lambda \simeq 20\,\mathrm{nm}$ (figure 5(c)) that, along with other EIT relevant characteristics (i.e. the group index of $\simeq$10 and 7, the loss of $\simeq$0.5 and $\simeq$0.3 dB per unit cell leading to the propagation length at $1/e$-level of $\simeq$0.87 and 1.74 μm), results in slightly larger values of the bandwidth-delay product amounting to $\tau\Delta f \simeq 0.39$ and 0.52 for the metamaterials with small and large unit cells, respectively. We should therefore add the unit cell composition to the list of optimization parameters formulated at the end of the previous section, bearing in mind that one can certainly come up with many other configurations complying with the general DED principle. Note that the inter-dipole interactions and thereby the positions and even orientations of scatterers are also important, influencing the *exact* position and depth of the minimum in the extinction spectrum as well as the resulting group index and loss dispersion of metamaterials.

4. DED metamaterials using gold nanorods

Metamaterials utilizing silver nanoparticles in air might be very difficult to realize in practice, and our choice of the metamaterial composition considered above was primarily dictated by the general interest in direct comparison of the DED configurations with that based on strongly coupled radiative and dark elements [12]. Moreover, the electrostatic approximation and point-dipole approach used in section 3 to calculate the response of the unit cell become questionable for larger particles that are more accessible for fabrication. In the following, we consider similar configurations consisting of gold nanorods embedded in glass ($n = 1.45$) and compute the cell responses with the finite-element method (FEM) implemented in the commercial software

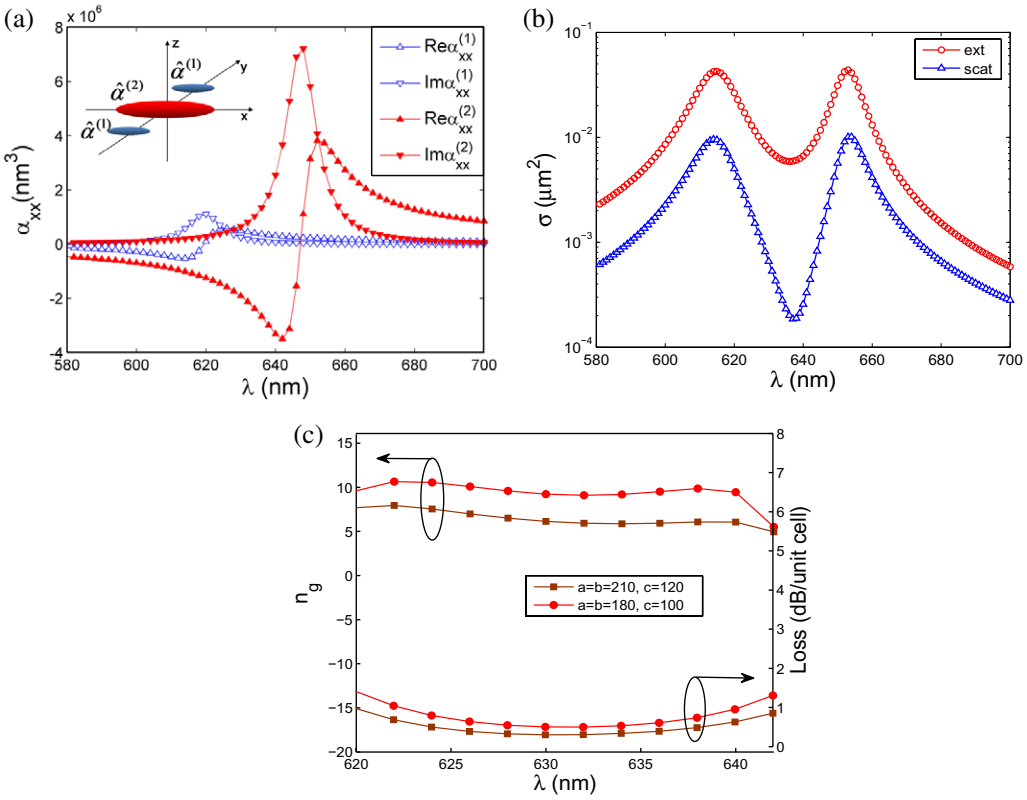

Figure 5. (a) Real and imaginary parts of polarizabilities of individual silver ellipsoids (in air) with sizes $40.9 \times 8.2 \times 8.2$ and $73.9 \times 13.7 \times 13.7\,\text{nm}^3$ (center-to-center distance of 90 nm), comprising the cell of type II (see inset). (b) Extinction and scattering cross sections of the single DED cell of type II calculated for the x-polarized light incident along the z-axis, with all dipole interactions being taken into account. (c) The corresponding dispersion of the group refractive index and loss per unit cell for DED-based metamaterials of type II for two different unit cells (a, b and c in the inset indicate the cell dimensions in nanometers along the x-, y- and z-axis, respectively).

COMSOL using a plane linearly polarized wave as a source and solving for the scattered field [26]. The nanorods were surrounded by a spherical surface truncating the simulation domain, whose size was typically ∼500 nm, enclosed with the perfect matching layer that suppresses artificial reflections by the simulation domain boundary. The height of all nanorods was chosen to be 50 nm (so that, in practice, structures could be fabricated by applying one-step lithography to a 50-nm-thick gold film), with the nanorod resonances being tuned by adjusting their lengths [31].

4.1. Two-nanorod DED configuration

We start again with the simplest configuration (type I), in which the unit cell is represented by a pair of gold nanorods of different lengths (figure 6(a)) chosen in order to realize, for x-polarized light, properly detuned resonances in the near-infrared wavelength range

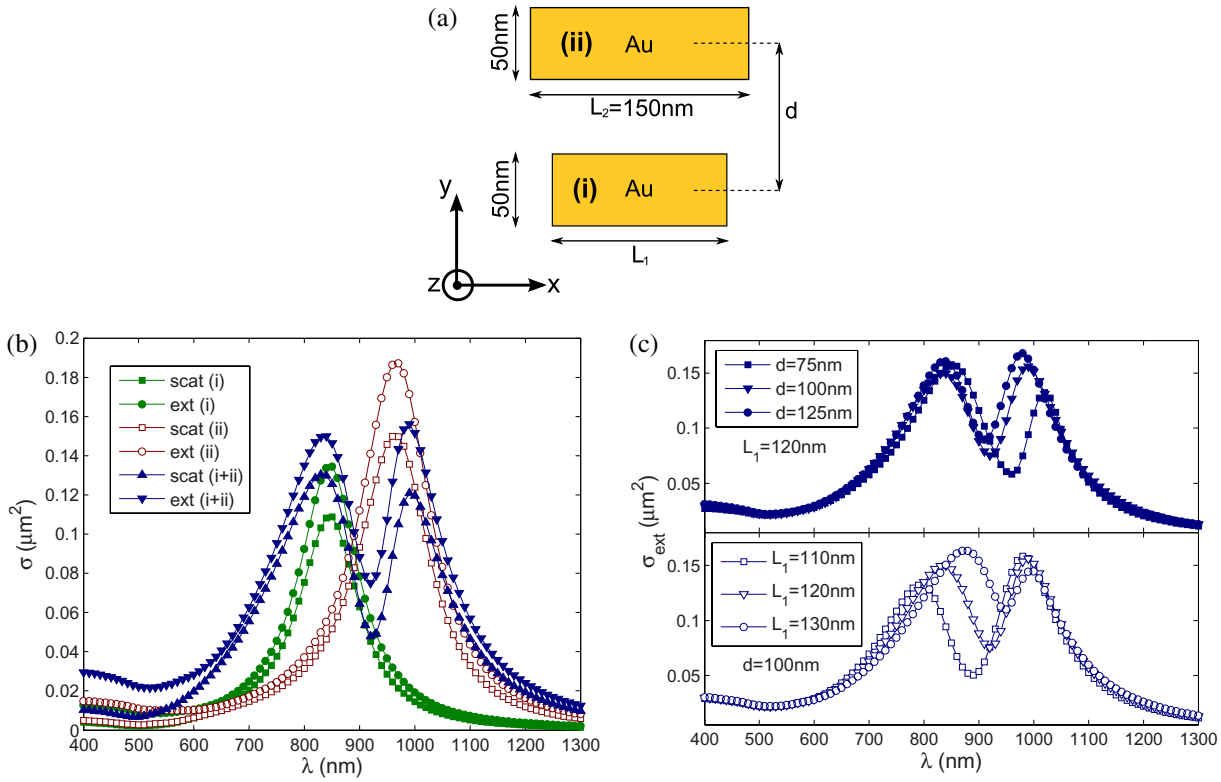

Figure 6. (a) Geometry of the two-nanorod configuration (type I), with the nanorod height (i.e. the dimension along the z-axis) being 50 nm. (b) Scattering and extinction spectra calculated for the individual 120- and 150-nm-long gold nanorods along with those for their composition into a single DED cell (center-to-center distance $d = 100$ nm) illuminated with x-polarized light. (c) Extinction spectra calculated for single DED cells of type I when varying the center-to-center distance d and the length L_1 of a shorter nanorod near their nominal values: $d = 100$ nm and $L_1 = 120$ nm.

(figure 6(b)). Comparing the DED cell (type I) spectra for silver nanoparticles (figure 2) and gold nanorods (figure 6(b)), one notices first of all that the resonances are much broader in the latter case, being influenced by both an increase in metal absorption (silver is a better metal than gold at optical frequencies [30]) and usage of glass as the surrounding dielectric medium (increasing thereby the field penetration in the metal). It is also seen that, contrary to the former, the scattering and extinction cross sections are quite similar in the latter case. This feature can be related to a considerable increase in the volume of scatterers, because the relative contribution of scattering (to the extinction) increases with the volume of scatterers [28]. Such a trend could have been considered positive from the perspective of EIT realization (since it implies a decrease of absorption contribution) but for the fact that the scattering suppression is not so deep as with ellipsoid nanoparticles. We believe that this (surprising) feature is related to the following circumstance: while the EIT mechanism relies on (electric) dipole interactions, scattering by larger particles becomes less dipole like, containing progressively stronger contributions from other multipoles (e.g. electrical quadrupoles and magnetic dipoles). In fact, the concept of particle polarizability used for the qualitative consideration of EIT with plasmonic nanoparticles

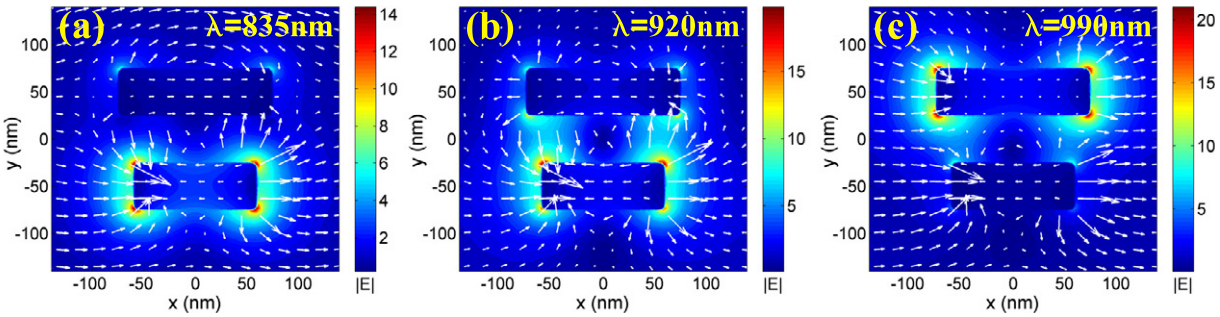

Figure 7. Normalized (to the incident field) electric-field magnitude distributions in the middle plane of nanorods with nominal dimensions calculated for different wavelengths $\lambda = 835$ (a), 920 (b) and 990 nm (c) of the x-polarized incident light.

(section 2) becomes less and less applicable for larger particles. It is, however, seen that the *general* behavior of scattering and extinction spectra is EIT like and quite similar in both cases (cf figures 2 and 6(b)). Moreover, this behavior is stable with respect to variations in both the length and the separation of DED scatterers (figure 6(c)) in line with the discussion in section 2.

The underlying electrodynamics involved in the scattering suppression by DED structures is illustrated by the electric field distributions in the x–y plane cutting through the middle of nanorods (with nominal dimensions: $d = 100$ nm, $L_1 = 120$ nm and $L_2 = 150$ nm) calculated for different wavelengths (figure 7). It is seen that at the wavelengths of 835 and 990 nm associated with the resonances of the individual nanorods (figure 6(b)), electromagnetic excitations are almost exclusively located at the corresponding nanorods (figures 7(a) and (c)). At the central DED wavelength of 920 nm, however, both nanorods are excited featuring *oppositely* induced electric dipoles (figure 7(b)). The *net* electric dipole moment is thereby greatly reduced, resulting in the suppression of scattering and extinction (figure 7(b)). Note that, *fundamentally*, this physical mechanism responsible for the EIT-like extinction spectra is analogous to the excitation of the so-called trapped mode formed by counter-propagating currents in the fish-scale [13], double-ring [16] and asymmetrically split ring [32] structures investigated in the cm-wavelength range. At the same time, the electric fields induced in the nanorods at the DED wavelength (figure 7(b)) indicate the occurrence of an induced magnetic dipole similar to that appearing in the asymmetrically split ring structures [32], a feature that suggests other (than optical transparency) interesting physical phenomena, such as optical activity [33] and spectral collapse [34].

4.2. Three-nanorod DED configuration

Following the line of reasoning of section 3, we consider here the three-nanorod DED configuration (type II) of a unit cell (figure 8(a)). It is seen that both scattering and extinction spectra calculated for this configuration bear a close resemblance to those obtained for the two-nanorod (type I) configuration (cf figures 6 and 8) and to the spectra of type II configuration with silver nanoparticles (figure 5(b)), albeit the latter exhibit considerably narrower resonances, as discussed in section 4.1. It should be noted that, to balance the scattering strengths of one longer nanorod and two shorter nanorods, the latter were designed to be narrower and shorter

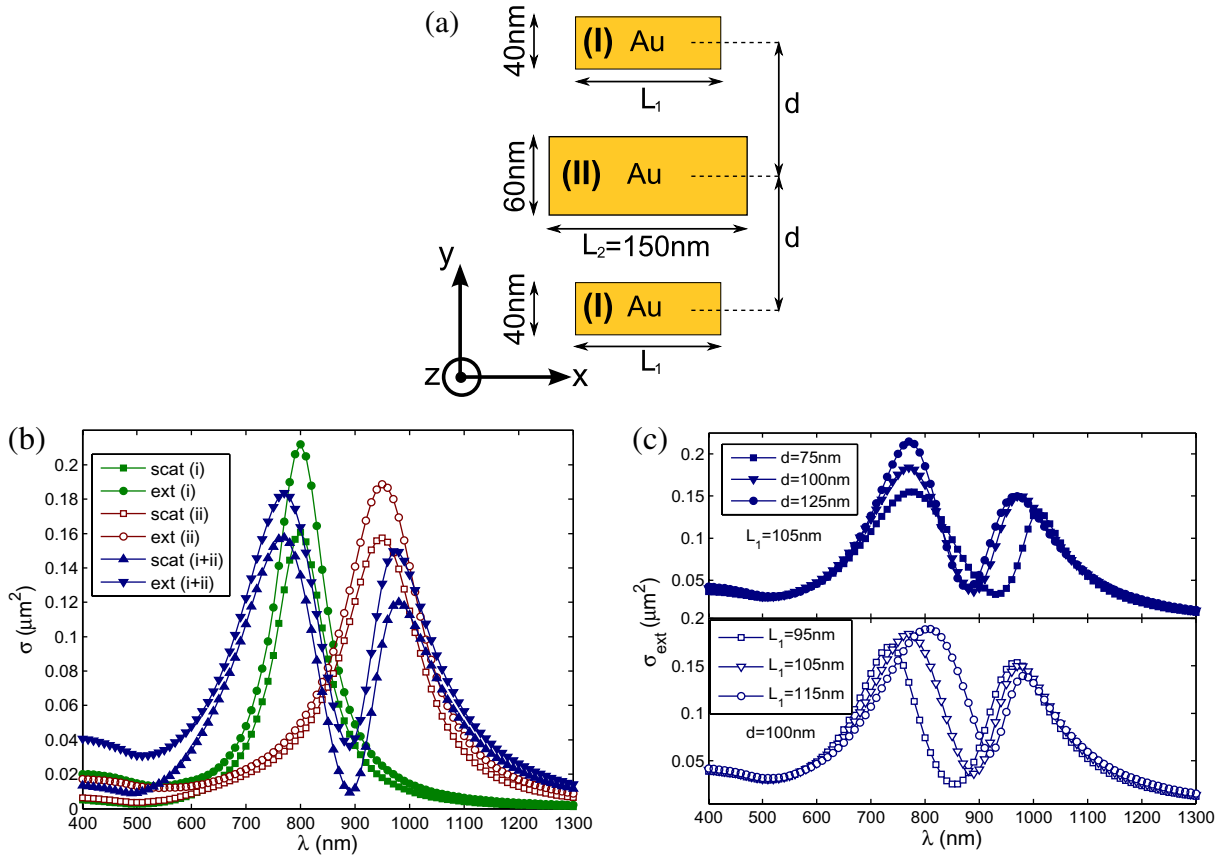

Figure 8. (a) Geometry of the three-nanorod configuration (type II) with the nanorod height (i.e. the dimension along the z-axis) being 50 nm. (b) Scattering and extinction spectra calculated for the individual 105- and 150-nm-long gold nanorods along with those for their composition into a single DED cell (center-to-center distances $d = 100$ nm) illuminated with x-polarized light. (c) Extinction spectra calculated for single DED cells of type II when varying the center-to-center distance d and the length L_1 of shorter nanorods near their nominal values: $d = 100$ nm and $L_1 = 105$ nm.

than the short nanorod in the unit cell of type I, resulting in a blue-shift of the short-wavelength resonance (i.e. from $\simeq$825 to 770 nm) and in deeper extinction and scattering minima at the central DED wavelength of $\simeq$890 nm (figure 8(b)). Here, we would like to again emphasize that the optimization of DED unit cells requires a very careful consideration of several parameters, as discussed in section 3. For example, it is clear that the transmission at the central DED wavelength improves for larger detuning Δ that can, on the other hand, result in deterioration of the slow-light effect. Finally, it is worth noting that the extinction and scattering spectra calculated for different nanoparticles (silver and gold) and cell compositions (types I and II) are similar, showing the EIT-like behavior.

The electric field distributions in the x–y plane cutting through the middle of nanorods (with nominal dimensions: $d = 100$ nm, $L_1 = 120$ nm and $L_2 = 105$ nm) calculated for different wavelengths exhibit physical effects (figure 9) similar to the previous case (figure 7): at the wavelengths of 770 and 975 nm associated with the resonances of the individual nanorods

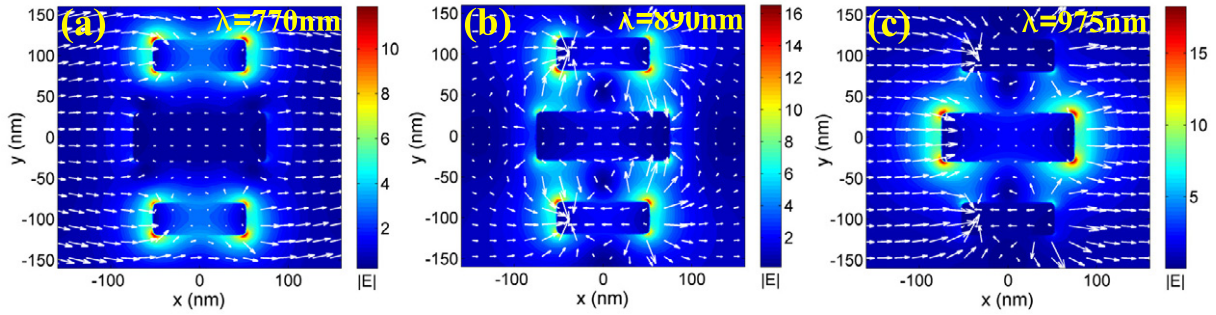

Figure 9. Normalized (to the incident field) electric-field magnitude distributions in the middle plane of nanorods with nominal dimensions calculated for different wavelengths $\lambda =$ (a) 770, (b) 890 and (c) 975 nm of the x-polarized incident light.

(figure 8(b)), electromagnetic excitations are almost exclusively located at the corresponding nanorods (figures 9(a) and (c)), whereas at the central DED wavelength of 890 nm, all nanorods are excited featuring *oppositely* induced electric dipoles (figure 9(b)). The *net* electric dipole moment is thereby greatly reduced at the DED wavelength, resulting in the suppression of scattering and extinction (figure 8(b)). Note that, *contrary* to the previous case, the electric fields in the nanorods at the DED wavelength (figure 9(b)) do *not* induce a magnetic dipole (only a magnetic quadrupole), a feature that is similar to the behavior of double-ring structures (and unlike asymmetrically split ring structures) and that suggest thereby a relatively weak dependence of the transmission on the angle of incidence [16].

4.3. Nanorod-based DED metamaterials

The procedure of calculation of the effective refractive index for DED-based metmaterials was considered in detail in section 3. It was demonstrated that, similar to the work [12], the effective index can be determined using the transmission spectrum obtained even with a monolayer of unit cells (figure 3(b)). The transmission and reflection spectra calculated for one layer of unit cells of type I and II, consisting of gold nanorods (with the nominal dimensions) illuminated with x-polarized light, exhibit the EIT-like transmission spectra with windows of transparency at the DED wavelengths of ∼900 and 870 nm, respectively (figure 10(a)) and quite strong reflection away from the DED wavelengths, at which it is strongly suppressed (figure 10(b)). The fact that (at the DED wavelengths) the reflection suppression is virtually complete while the transparency is not agrees well with our general consideration of EIT realization with plasmonic nanostructures presented in the introduction. It is also seen that the transmission and reflection spectra are rather asymmetric with respect to the transparency window. We think that, apart from the Rayleigh scaling of the scattering strength with wavelength that can be also noted with silver nanoparticles (figure 3(a)), the contribution from multipoles discussed above becomes progressively more important for shorter wavelengths.

The transmission and reflection spectra calculated for three layers of unit cells were used to determine the dispersion of the corresponding metamaterial effective refractive indexes [35]. Note the similarity of the dispersion of real and imaginary parts of the effective index (figure 10(c)) to that obtained for the metamaterials using silver nanoparticles (figure 4(a)). The group refractive index and loss (per cell thickness) for different metamaterials (types I

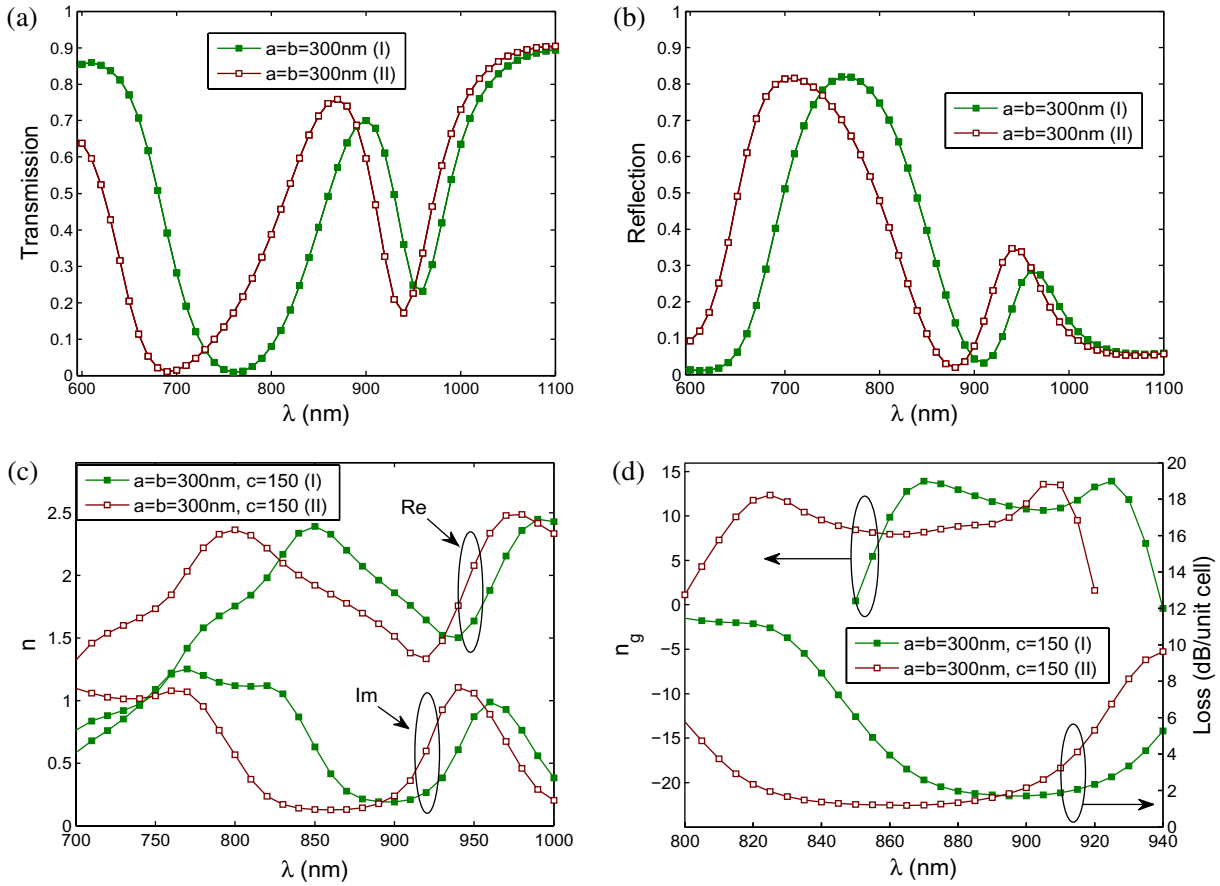

Figure 10. (a) Transmission and (b) reflection spectra calculated for one layer of unit cells (a, b and c in the insets indicate the cell dimensions in nanometers along the x-, y- and z-axes, respectively) of types I and II consisting of the gold nanorods (with nominal dimensions) illuminated with x-polarized light. (c) Dispersion of the refractive (real and imaginary parts) index of metamaterials of types I and II calculated directly from the transmission and reflection by three layers of unit cells. (d) The corresponding dispersion of the group index and loss per unit cell for DED-based metamaterials using gold nanorods embedded in glass.

and II) were straightforwardly evaluated from the corresponding dispersion (figure 10(d)). Since the group velocity is meaningful only in the domain of normal dispersion with relatively small absorption [28], these dependences should be considered only in the wavelength range of ∼860–935 nm (type I) and ∼810–915 nm (type II). We are now in a position to evaluate (as was done in section 3) the corresponding metamaterial characteristics relevant to the EIT effect for both (types I and II) configurations: the group index $n_g \simeq 11$ and 8, the transparency bandwidth $\delta\lambda \simeq 60$ and 70 nm centered at the wavelengths $\lambda \simeq 900$ and 870 nm, the propagation loss of $\simeq 2$ and 1 dB per 150-nm-thick unit cell resulting in the propagation lengths $L \simeq 0.33$ and 0.65 μm, respectively. Using these data, one can also estimate the bandwidth-delay product $\tau\Delta f \simeq \lambda^{-2}\delta\lambda L(n_g - 1.5) \simeq 0.23$ and 0.39, both values being similar to those calculated above for the DED-based metamaterials using silver nanoparticles operating at shorter wavelengths, so

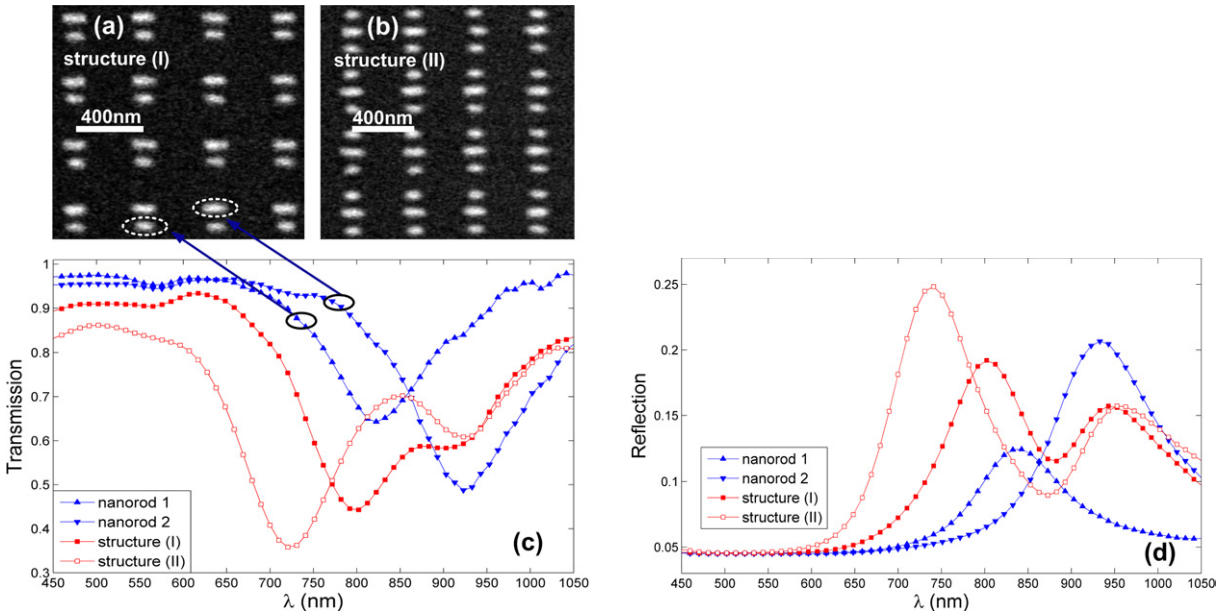

Figure 11. Electron microscopy images of fabricated 400-nm-period arrays consisting of gold nanorods separated by gaps of ∼50 nm and being ∼50 × 55 nm^2 in cross section with lengths of approximately (a) 90 and 135 nm and (b) 115 and 145 nm. (c) Transmission and (d) reflection spectra for the fabricated structures including the reference spectra for the arrays of individual 100- and 140-nm-long nanorods.

that an increase in absorption when using gold instead of silver is somewhat compensated for by a decrease in absorption when increasing the light wavelength. Finally, it should be emphasized that, in both the cases considered, the geometrical parameters of ellipsoids and nanorods (as well as their separations and unit cell sizes used) were not optimized with respect to achieving the best performance with respect to the bandwidth-delay product, which is a very important characteristic [3]. Our *main* intention was to demonstrate an alternative, DED-based approach to the plasmon-induced optical transparency [12, 15] as well as its attractive features of robustness and versatility.

5. Preliminary experiments

To experimentally demonstrate the suggested approach for optical transparency, we fabricated 400-nm-period arrays (50 × 50 μm^2) consisting of individual, double and triple gold nanorods on a silica substrate using electron-beam lithography and lift-off applied to a 50-nm-thick gold film (figures 11(a) and (b)). Note that the fabricated nanorods exhibit noticeable variations in size and shape, indicating that the fabrication procedure has to be further developed and optimized to achieve better quality and reproducibility of nanorod arrays. The fabricated sample was subsequently covered with a ∼15-μm-thick (index-matching) layer of poly(methyl methacrilate), i.e. PMMA. Transmission spectra were measured using a broadband halogen light source with a fiber output whose (weakly divergent) radiation was directed (at normal incidence) through a polarizer on the fabricated arrays of nanorods aligned so that their axes were parallel

to the light polarization. The transmitted radiation was collected with an objective, directed through an analyzer (oriented parallel to the polarizer) and fed into an optical fiber connected to a spectrometer. The reflection spectra of the fabricated arrays were obtained in a similar manner except that the incident polarized light was focused onto the sample by an objective with a numerical aperture of 0.85 and 60× magnification. The reflected light from the fabricated arrays was collected by the same objective, sent through an analyzer and subsequently fed into the optical fiber connected to the spectrometer. The transmission spectra were further normalized using the sample transmission measured outside the arrays of nanorods, whereas the reflection spectra were normalized using reflection measurements with a 300-nm-thick gold film weighted with the calculated reflectivity [30].

The transmission and reflection spectra obtained with arrays of individual short and long nanorods exhibit the effect of detuning in their resonances located at $\simeq$820 and 920 nm, while the transmission spectrum of the array consisting of a pair of corresponding nanorods (figure 11(a)) shows a slightly increased transmission at the intermediate (DED) wavelength of $\simeq$870 nm (figure 11(c)). We believe that this effect is weak because the detuning in resonances of *fabricated* nanorods turned out to be too small with respect to the widths of individual resonances. A considerably better pronounced effect of the increased transmission at the DED wavelength of $\simeq$850 nm is seen in the spectrum measured for the array of triplets of nanorods (figure 11(b)), most probably because of more suitable detuning in this case. It should be borne in mind that the use of divergent illumination and detection of focused radiation as well as inhomogeneous broadening (due to fabrication-induced deviations of nanorod dimensions in the fabricated arrays) could definitely contribute to smearing out the desirable effect of transparency in these *preliminary* experiments.

For both configurations, the reflection spectra exhibit maxima at the resonance wavelengths of individual nanorods and minima at the DED wavelengths (figure 11(d)), with the latter being noticeably better pronounced than the corresponding transmission maxima. The fact that the EIT-like behavior is more prominent in the reflection than in transmission spectra supports further our previous arguments and discussions in the introduction and in section 4.3. In general, the experimentally measured spectra (figures 11(c) and (d)) resemble the spectra calculated for gold nanorods in section 4.3 (figures 10(a) and (b)), featuring, for example, similar asymmetry with respect to the transparency window related above to the Rayleigh scaling of scattering strength and contribution of multipoles. Taking into account the aforementioned fabrication imperfections along with noticeable differences in shape of model (i.e. rectangular prism-like) nanorods and fabricated particles (figures 11(a) and (b)), we decided to abstain from purposefully fitting modeling to experimental spectra. We believe that a qualitative comparison of the main trends and features that revealed reasonable agreement is sufficient for the purpose of this work introducing the DED-based approach to plasmon-induced transparency.

6. Conclusions

Summarizing, we have suggested a novel type of optical metamaterial whose unit cells consist of electric dipolar scatterers resonating at *different* frequencies (DED) and thereby only weakly interacting (in contrast to resonant unit cells considered in [36]). We have presented qualitative arguments supported by numerical modeling of DED configurations consisting of silver nanoparticles in air, demonstrating the *fundamental equivalence* of two approaches to plasmon-induced optical transparency, namely those relying on the bare- and dressed-state

Table 1. Main characteristics of the simulated DED configurations.

DED system	λ (nm)	Cell size (nm^3)	$\delta\lambda$ (nm)	Loss (dB per cell)	n_g	$\tau\Delta f$
Type I (silver/air)	633	$210 \times 210 \times 120$ ($150 \times 150 \times 90$)	15 (13)	0.3 (0.6)	7 (14)	0.39 (0.27)
Type II (silver/air)	633	$210 \times 210 \times 120$ ($180 \times 180 \times 100$)	20 (20)	0.3 (0.5)	7 (10)	0.52 (0.39)
Type I (gold/glass)	900	$300 \times 300 \times 150$	60	2	11	0.23
Type II (gold/glass)	870	$300 \times 300 \times 150$	70	1	8	0.39

pictures of EIT. We have further considered, both theoretically and experimentally, DED configurations based on gold nanorods embedded in a polymer exhibiting the effect of optical transparency at wavelengths of $\sim$850 nm, and illustrated two very important features of it: *versatility* (different configurations of unit cells consisting of different numbers of scatterers can be used) and *robustness* with respect to mutual positioning of individual scatterers (inside the cell). The bandwidth-delay product evaluated numerically for the considered configurations was found to vary in the range of 0.23–0.52 (table 1), values that are favorably comparable to that calculated using the plasmonic CRIT principle [11]. Note that we also succeeded in the experimental demonstration of EIT-like behavior (increased transmission accompanied by suppression of scattering) at close to visible wavelengths that are much shorter than those employed in recent experiments on the plasmon-induced EIT [15, 37].

We would like to stress that even though the inter-dipole interactions (and thereby the positions of scatterers) are important, influencing the exact position and depth of the minimum in the extinction spectrum as well as the resulting dispersion of metamaterial, the general EIT-like behavior and the decrease in group velocity (in the domain of normal dispersion) are only weakly affected, especially for sufficiently large detunings that are close to that given by the optimum condition. Note that the condition of optimum detuning obtained in the approximation of non-interacting dipolar scatterers should be considered only as an estimate, with a careful optimization to be conducted for a given DED configuration designed to operate in a given frequency range. We are carrying out further investigations, calculating the optimum parameters for nanorod-based arrays and improving the fabrication procedure. Finally, we would like to emphasize that the DED-based metamaterials can be implemented with other compositions of plasmonic resonant scatterers with different configurations, e.g. represented by metal nanoshells of different thicknesses, radii and/or dielectric cores [21], a configuration that is expected to be virtually isotropic in its optical response.

Acknowledgments

We acknowledge financial support for this work from the VELUX Foundation and from the Danish Council for Independent Research (the FTP project ANAP, contract no. 09-072949).

References

[1] Boller K J, Imamoglu A and Harris S E 1991 *Phys. Rev. Lett.* **66** 2593–6
[2] Fleischhauer M, Imamoglu A and Marangos J P 2005 *Rev. Mod. Phys.* **77** 633–73
[3] Krauss T F 2008 *Nat. Photonics* **2** 448–50
[4] Maleki L, Matsko A B, Savchenkov A A and Ilchenko V S 2004 *Opt. Lett.* **29** 626–8
[5] Smith D D, Chang H, Fuller K A, Rosenberger A T and Boyd R W 2004 *Phys. Rev.* A **69** 063804
[6] Yanik M F, Suh W, Wang Z and Fan S 2004 *Phys. Rev. Lett.* **93** 233903
[7] Xu Q, Sandhu S, Povinelli M L, Shakya J, Fan S and Lipson M 2006 *Phys. Rev. Lett.* **96** 123901
[8] Totsuka K, Kobayashi N and Tomita M 2007 *Phys. Rev. Lett.* **98** 213904
[9] Yang X, Yu M, Kwong D-L and Wong C W 2009 *Phys. Rev. Lett.* **102** 173902
[10] Miroshnichenko A E, Flach S and Kivshar Y S 2010 *Rev. Mod. Phys.* **82** 2257–97
[11] Kekatpure R D, Barnard E S, Cai W and Brongersma M L 2010 *Phys. Rev. Lett.* **104** 243902
[12] Zhang S, Genov D A, Wang Y, Liu M and Zhang X 2008 *Phys. Rev. Lett.* **101** 047401
[13] Papasimakis N, Fedotov V A, Zheludev N I and Prosvirnin S L 2008 *Phys. Rev. Lett.* **101** 253903
[14] Tassin P, Zhang L, Koschny T, Economou E N and Soukoulis C M 2009 *Phys. Rev. Lett.* **102** 053901
[15] Liu N, Langguth L, Weiss T, Kästel J, Fleischhauer M, Pfau T and Giessen H 2009 *Nat. Mater.* **8** 758–62
[16] Papasimakis N, Fu Y H, Fedotov V A, Prosvirnin S L, Tsai D P and Zheludev N I 2009 *Appl. Phys. Lett.* **94** 211902
[17] Luk'yanchuk B, Zheludev N I, Maier S A, Halas N J, Nordlander P, Giessen H and Chong C T 2010 *Nat. Mater.* **9** 707–15
[18] Baba T 2008 *Nat. Photonics* **2** 465–73
[19] Maier S A 2009 *Nat. Mater.* **8** 699–700
[20] Evlyukhin A B, Bozhevolnyi S I, Pors A, Nielsen M G, Radko I P, Willatzen M and Albrektsen O 2010 *Nano Lett.* **10** 4571–7
[21] Prodan E, Radloff C, Halas N J and Nordlander P 2003 *Science* **302** 419–22
[22] Sönnichsen C, Franzl T, Wilk T, von Plessen G, Feldmann J, Wilson O and Mulvaney P 2002 *Phys. Rev. Lett.* **88** 077402
[23] Jylhä L, Kolmakov I, Maslovski S and Tretyakov S 2006 *J. Appl. Phys.* **99** 043102
[24] Wang F and Shen Y R 2006 *Phys. Rev. Lett.* **97** 206806
[25] Della Valle G, Søndergaard T and Bozhevolnyi S I 2009 *Phys. Rev.* B **80** 235405
[26] Pors A, Willatzen M, Albrektsen O and Bozhevolnyi S I 2010 *J. Opt. Soc. Am.* B **27** 1680–7
[27] Yariv A 1989 *Quantum Electronics* 3rd edn (New York: Wiley)
[28] Jackson J D 1999 *Classical Electrodynamics* 3rd edn (New York: Wiley)
[29] Evlyukhin A B and Bozhevolnyi S I 2005 *Surf. Sci.* **590** 173–80
[30] Johnson P B and Christy R W 1972 *Phys. Rev.* B **6** 4370–9
[31] Nielsen M G, Pors A, Nielsen R B, Boltasseva A, Albrektsen O and Bozhevolnyi S I 2010 *Opt. Express* **18** 14802–11
[32] Fedotov V A, Rose M, Prosvirnin S L, Papasimakis N and Zheludev N I 2007 *Phys. Rev. Lett.* **99** 147401
[33] Plum E, Liu X-X, Fedotov V A, Chen Y, Trsai D P and Zheludev N I 2009 *Phys. Rev. Lett.* **102** 113902
[34] Fedotov V A, Papasimakis N, Plum E, Bitzer A, Walther M, Kuo P, Tsai D P and Zheludev N I 2010 *Phys. Rev. Lett.* **104** 223901
[35] Smith D R, Schultz S, Markoš P and Soukoulis C M 2002 *Phys. Rev.* B **65** 195104
[36] Cai W and Shalaev V 2010 *Optical Metamaterials* (New York: Springer)
[37] Zhang J, Xiao S, Jeppesen C, Kristensen A and Mortensen N A 2010 *Opt. Express* **18** 17187–92